



Cite this: *Phys. Chem. Chem. Phys.*,
2017, **19**, 26369

Theoretical study on geometric, electronic and catalytic performances of Fe dopant pairs in graphene†

Yanan Tang,^{‡*} Huadou Chai,^a Weiguang Chen,^{‡*} Xiao Cui,^a Yaqiang Ma,^{‡*} Mingyu Zhao^b and Xianqi Dai^{*ab}

The formation geometries, electronic structures and catalytic properties of monovacancy and divacancy graphene sheets with two embedded Fe dopants (2Fe-MG and 2Fe-DG) have been systematically investigated using the first-principles calculations. It was found that the configuration of 2Fe-DG is slightly more stable than that of 2Fe-MG sheets and the two doped Fe atoms in graphene (2Fe-graphene) as active sites could regulate the stability of gas molecules. In addition, the adsorption of O₂ and CO molecules could modulate the electronic and magnetic properties of 2Fe-graphene systems. Moreover, the adsorption behaviors of reactants could determine the reaction pathway and energy barrier of the catalytic oxidation of CO. On the 2Fe-graphene substrates, the adsorptive decomposition of O₂ molecules (<0.20 eV) and the subsequent Eley–Rideal (ER) reaction (2O_{ads} + 2CO → CO₂) (<0.60 eV) have low energy barriers. In comparison, the CO₃ complex is quite stable and its formation needs to overcome a higher energy barrier (>0.90 eV). Hence, the dissociation of O₂ as an initial step is an energetically more favored process. These results provide valuable guidance for the design of functionalized graphene-based devices.

Received 20th August 2017,
Accepted 6th September 2017

DOI: 10.1039/c7cp05683d

rsc.li/pccp

1. Introduction

The catalytic oxidation of CO has attracted great interest because CO, which is emitted from automobiles and industrial production, represents a significant environmental problem.^{1–3} In recent years, CO oxidation has been viewed as the most important chemical reaction for studying the reactivity of catalysts.^{4–6} Many studies have chosen metal clusters supported on noble metal or metal oxide (such as TiO₂, MgO and FeO_x) substrates^{7–13} or even unsupported metal nanoparticles,^{14–16} which exhibit high catalytic activity for CO oxidation. The size of the metal particles is a key factor that determines the performance of such catalysts, because low-coordinated metal atoms often function as the catalytically active sites, and the specific activity per metal atom usually increases with a decrease in the size of the metal particles.^{17,18} To maximize the catalytic efficiency, it is desirable to shrink supported metal particles to isolated single atoms uniformly dispersed on a substrate. Recently,

metal catalysts supported on a two-dimensional hexagonal boron nitride (BN) monolayer^{19–21} have exhibited high activity for CO oxidation. In comparison with traditional supports,²² the use of graphene as a support with its high surface area, good conductivity and low manufacturing cost has been proposed to modulate the electronic structure and hence improve the catalytic performance of supported catalysts.^{23–25} Some results have shown that Au and Pt metal clusters supported on graphene could effectively catalyze CO oxidation.^{26,27} However, the surface free energy of metals increases significantly with a decrease in particle size, which promotes the aggregation of small clusters; thus, the stability and reaction efficiency of catalysts will be affected.

Graphene is a promising candidate as a substrate for supported metal atoms or clusters to form graphene-metal composite catalysts.^{28,29} The adsorption of different metal adatoms on pristine graphene sheets³⁰ and the induced electronic and magnetic properties of graphene systems have been discussed *via* theoretical calculations.^{31–35} Owing to the weak interactions between metal adatoms and pristine graphene, adatoms tend to diffuse and aggregate to form large clusters instead of existing as individual atoms. In this context, chemical doping has been proved to be an effective approach for tailoring the functionalized properties of graphene.³⁶ The existence of vacancies in graphene could efficiently enhance the binding of metal atoms, which has a substantial effect on the electronic and magnetic properties of graphene.^{37–39} In particular, it is possible to dope metallic impurities in graphene

^a Quantum Materials Research Center, College of Physics and Electronic Engineering, Zhengzhou Normal University, Zhengzhou 450044, China.
E-mail: yntang2010@163.com; Fax: +86 371 65501661; Tel: +86 371 65501661

^b College of Physics and Materials Science, Henan Normal University, Xinxiang 453007, China. E-mail: xqdaizs@163.com

† Electronic supplementary information (ESI) available. See DOI: 10.1039/c7cp05683d

‡ These authors contributed equally to this article and are considered co-first authors.

by using electron irradiation or high-energy atom bombardment and then fill the vacancies with the desired dopants.^{40,41} Hence, the high stability of metallic impurities in graphene sheets could make them better candidates for improving the dispersion and extending the lifetime of supported catalysts. Moreover, some theoretical studies found that graphene systems with single embedded metal atoms (Cu, Pt, Co, Au and Al) exhibited high catalytic performance for low-temperature CO oxidation.^{42–47} These observations confirmed that different dopants could modify the local surface curvature and electronic properties of graphene and thus regulate its chemical activity.^{48,49}

Many studies have found that metal dimers (Fe, Au, Co, Ni, Pd and Cu) supported on graphene sheets could give rise to interesting new phenomena, such as electronic and magnetic properties.^{50–53} In catalytic reactions, bimetallic nanoclusters and metal dimer catalysts supported on CeO₂ substrates exhibit high activity for CO oxidation.^{54,55} Recently, the adsorption and dissociation of O₂ on yttria-stabilized zirconia (YSZ) surfaces with supported Ni dimers have been investigated.⁵⁶ The results illustrated that the large number of active sites of supported metal dimers could exhibit high activity and greatly enhance the interaction between reactants and catalysts through an increase in the transfer of electrons. At present, the single-atom Fe embedded monovacancy⁵⁷ and divacancy⁵⁸ graphene, C₂N monolayers⁵⁹ and anchored graphene oxide⁶⁰ systems, which exhibit high catalytic activity for CO oxidation, have been investigated. However, there has been a lack of systematic analyses of the geometric stability and catalytic properties of two Fe atoms supported on a graphene sheet (2Fe-graphene).

Recently, some researchers have investigated covalently bonded Fe dopants in the lattice of monolayer graphene, which are more stable than those at graphene edges.⁶¹ On the basis of single Fe atoms in graphene vacancies,⁶² we selected monovacancy and divacancy graphene sheets with two embedded Fe atoms (2Fe-MG and 2Fe-DG) and then investigated their catalytic activity for CO oxidation. First, the formation geometries, electronic structures and magnetic properties of 2Fe-MG (and 2Fe-DG) with adsorbed gases (CO and O₂) are discussed using first-principles calculations based on density functional theory (DFT). It was found that the transfer of more electrons to O₂ molecules on 2Fe-graphene sheets led to higher stability in comparison with that of adsorbed CO molecules. The electronic and magnetic properties of 2Fe-graphene systems could be effectively regulated by choosing different gas molecules. Moreover, the reaction processes and energy barriers of CO oxidation on the 2Fe-graphene surfaces were calculated using different reaction mechanisms. To the best of our knowledge, few reports provide much systematic information about the catalytic activity of two Fe atoms supported on graphene sheets (including MG and DG), which provides a valuable reference for the design of graphene-based catalysts in energy-related devices.

2. Methods and computational details

Spin-polarized DFT calculations were carried out using the Vienna *ab initio* simulation package (VASP)^{63,64} with projector

augmented wave (PAW) pseudopotentials.⁶⁵ Exchange–correlation functions were described using the generalized gradient approximation (GGA) in the form of the Perdew–Burke–Ernzerhof (PBE) functional.⁶⁶ The kinetic energy cutoff for the plane-wave basis set was chosen to be 450 eV. The C 2s and 2p, Fe 3d and 4s and O 2s and 2p states were treated as valence electrons. A modified hexagonal graphene ribbon with a 4 × 7 supercell was adopted, and the thickness of the vacuum layer was set to 15 Å to avoid interactions between mirror images. The calculated lattice constant of a graphene sheet was 2.47 Å, which closely approximates to the experimental value of 2.46 Å.⁶⁷ The Brillouin zone (BZ) integration was sampled using a 3 × 1 × 1 Γ -centered Monkhorst–Pack (MP) grid and a 15 × 1 × 1 Γ -centered MP grid was used for calculations of the final density of states (DOS).

Bader charge analysis⁶⁸ was used to evaluate the atomic charges and electron transfer in the reactions. The adsorption energies and site preferences of each type of gas molecule were determined on 2Fe-graphene sheets. The energy of an isolated atom was simulated using a cubic cell of 15 × 15 × 15 Å with one atom or gas molecule placed inside. The climbing image nudged elastic band method (CI-NEB)^{69,70} was employed to find the saddle points and minimum-energy path (MEP) for the formation and dissociation of reactants on graphene substrates. The geometry optimization and search for transition states (TS) were tested by means of frequency calculations, in which the states with one imaginary frequency corresponded to metastable states (MS). A number of intermediate images were constructed along the reaction pathways between the initial state (IS) or TS and the final state (FS), and the spring force between adjacent images was set to 5.0 eV Å⁻¹. The images were optimized until the forces on each atom were less than 0.02 eV Å⁻¹. The energy barrier (E_{bar}) of each chemical reaction was calculated from the energy difference between the IS and the TS in the chemical reaction.

In the present study, the binding energy (E_{bind}) was calculated using the equation $E_{\text{bind}} = E_{\text{A}} + E_{\text{B}} - E_{\text{AB}}$, where E_{A} , E_{B} and E_{AB} are the total energies of the free atom(s) or gas molecules (A, which represents Fe, O₂, O, CO or CO₂), the isolated 2Fe-graphene substrates (B, which represents MG, DG, 2Fe-MG or 2Fe-DG) and the 2Fe-graphene systems with the adsorbed molecules, respectively. With this definition, a positive (negative) value of the binding energy means that the adsorption process is exothermic (endothermic) and energetically favored (unfavored).

3. Results and discussion

3.1. Geometric properties of 2Fe-graphene sheets

Previous results have demonstrated that a two-step process is an efficient way to dope graphene, namely, by creating vacancies (including monovacancies and divacancies) in graphene by high-energy ion/electron irradiation and then filling these vacancies with the desired dopants.^{40,71} Herein, MG and DG act as trap sites created for individual Fe atoms to form covalently bonded Fe-MG and Fe-DG complexes, and the corresponding binding energies of the Fe dopant are 7.28 and 6.47 eV,

respectively, which are in agreement with the literature values.⁶² In the process, the trapping of the second Fe atom occurs subsequently to the initial formation of a single dopant site. For each MG (or DG) sheet, two Fe dopants are embedded in two adjacent monovacancies or an Fe dimer is trapped at a divacancy.⁶¹ The configurations of the two Fe dopants in MG and DG (2Fe-MG and 2Fe-DG) are shown in Fig. 1(a) and (b). As shown in Fig. 1(a), two Fe atoms are embedded in a DG sheet, where two C atoms are replaced by two Fe atoms. The lengths of the Fe–Fe and Fe–C bonds are 1.99 and 1.80 Å, respectively. The Fe dimer is displaced out of the plane to acquire more space (1.14 Å) due to its large atomic radius (1.30 Å) as compared with that of carbon atoms. On the basis of Bader charge analysis,⁶⁸ transferred electrons (1.41 *e*) move from the two Fe dopants to the DG sheet and then form strong covalent bonds between Fe and C atoms. As shown in Fig. 1(b), the stable configuration of 2Fe-MG was investigated after geometry optimization. In comparison with the 2Fe-DG system, the doped Fe atoms transfer more electrons (2.02 *e*) to the MG sheet because more neighboring carbon atoms bind to the Fe dopants, and the corresponding Fe–Fe and Fe–C bond lengths are 2.71 and 1.77 Å, respectively, which are in agreement with the reported results.^{37,57}

According to a previous result,⁷² we studied the relative stabilities of Fe-doped and 2Fe-doped graphene by comparing their formation energies (E_{form}) as calculated by the equation: $E_{\text{form}} = (E_{\text{D-gra}} + \mu_{\text{C}}) - (E_{\text{gra}} + \mu_{\text{Fe}})$, where E_{gra} is the total energy of pristine graphene, $E_{\text{D-gra}}$ is the total energy of the Fe–graphene system, and μ_{C} (or μ_{Fe}) is the chemical potential of an isolated

carbon (or Fe) atom, which is determined from graphene or the bulk metallic phase of Fe. The lower formation energy indicates that the adatom is more easily incorporated into the graphene sheet. Our results show that the formation energy of one Fe dopant within a monovacancy is 5.92 eV, which is higher than that of the second Fe dopant in MG (4.84 eV) and DG sheets (4.03 eV). This result illustrates that Fe dopants tend to be incorporated into the graphene sheet and that the 2Fe-DG sheet is an energetically more favored configuration.

As shown in Fig. 1(a) and (b), MG and DG act as trap sites for mobile Fe adatoms, which leads to the formation of 2Fe-MG and 2Fe-DG configurations. We also investigated the structural conversion between 2Fe-DG and 2Fe-MG sheets. It was found that the doped Fe atoms in an MG sheet exhibit lower stability than those in a DG sheet, and that 2Fe-MG is converted into the 2Fe-DG configuration through an energy barrier of 1.04 eV. In order to confirm the stability of the 2Fe-graphene systems, first-principles molecular dynamics calculations were considered. In calculations for a period of 2000 fs (2 ps) at temperatures of 700 K and 1000 K, the doped Fe atoms and the neighboring C atoms in the plane exhibit a slight distortion, as shown in Fig. S1(a)–(d) (ESI†). Although the hexagonal structure of graphene is bent to some extent, the 2Fe-graphene structures are still stable over a period of 2 ps at 1000 K, with some distortion over time. The corresponding Fe–Fe and Fe–C bond lengths are 2.62 and 1.70–1.90 Å (or 2.03 and 1.76–1.84 Å) for the 2Fe-MG (or 2Fe-DG) configuration, respectively. These results indicate that the two Fe atoms are immobile within defective graphene and that the

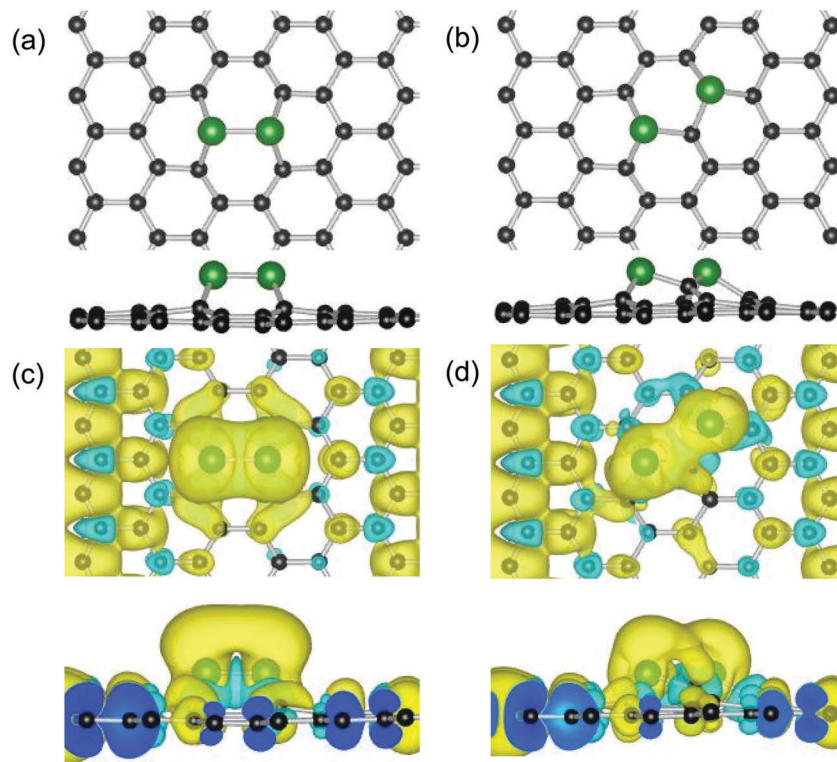


Fig. 1 Top and side views of (a and b) the geometric structure and (c and d) the spin charge density map of (a and c) 2Fe-DG and (b and d) 2Fe-MG sheets. The contour interval is $0.001 \text{ e} \text{ \AA}^{-3}$. The black and green balls represent C and Fe atoms, respectively.

2Fe-graphene sheets as active sites possess high thermal stability at certain temperatures, which has a profound effect on the use of the metal-graphene complexes as catalysts, gas sensors or energy-storage devices.

As shown in Fig. 1(c) and (d), we investigated the spin charge redistribution between the 2Fe dopants and the MG (or DG) sheets. It is clearly shown that more electrons predominantly accumulate in the vicinity of the Fe-Fe and Fe-C interfaces and that fewer electrons are located on the graphene sheets, as shown in Fig. 1(c). In comparison with the 2Fe-DG system, less pronounced charge density distributions are located at the Fe-Fe and Fe-C interfaces in the 2Fe-MG system, because more electrons are transferred from the Fe dopants to the MG sheet and thus enhance the interaction between the 2Fe dopants and the MG sheet. In addition, the transfer of electrons helps us to explain the change in magnetic properties and could affect the number of unpaired electrons in the graphene system. As shown in Fig. 1(c) and (d), the more pronounced spin charge distribution illustrates that the 2Fe-DG system exhibits stronger magnetic properties ($14.0 \mu_B$), whereas the 2Fe-MG system, which has a less pronounced spin charge distribution, has weaker magnetic properties ($12.0 \mu_B$), because a large number of transferred electrons saturate the neighboring dangling bonds of carbon atoms and decrease the number of unpaired electrons in the 2Fe-MG system. Hence, the metal dopant tends to transfer electrons to graphene and induces spin charge redistribution at their interface, thus regulating the magnetic properties of 2Fe-graphene systems.

3.2. Adsorption stability of gas molecules

On the basis of the stable configurations of 2Fe-MG and 2Fe-DG, the Fe dopants lose more electrons and exhibit positive charges, which could regulate the adsorption behaviors of gas molecules. Each structure was fully relaxed and the most stable configurations of the adsorbed species on the 2Fe-graphene substrate were studied, as shown in Fig. 2. The calculated energies, number of transferred electrons and bond lengths are shown in Table 1. It was found that the binding energies (E_{bind}) of an individual O_2 molecule (3.25 and 3.67 eV) on the 2Fe-graphene substrates are much higher than those of a CO molecule (1.43 and 1.72 eV). As shown in Fig. 2(a) and (c), an adsorbed O_2 molecule is parallel to the Fe-Fe bond and forms two O-Fe chemical bonds with a high E_{bind} value (> 3.0 eV), whereas an adsorbed CO molecule is nearly vertical in a bridging position with respect to the Fe-Fe bond. Besides, individual CO and O_2 molecules have higher energies on a 2Fe-MG sheet than on a 2Fe-DG substrate.

As shown in Fig. 2(a), the configuration of an O_2 molecule on a 2Fe-DG sheet has an E_{bind} value of 3.25 eV. About 1.02 electrons are transferred from the substrate to the O_2 molecule, which subsequently leads to an elongation of the O-O bond (1.47 Å). In comparison, an adsorbed O_2 molecule gains more electrons (1.06 e) on a 2Fe-MG sheet, and thus the O-O bond length increases to 1.48 Å. Hence, the elongation of the O-O bond is correlated with the amount of electronic charge transferred to the O_2 molecule; in other words, more the charge transferred from the 2Fe-graphene system to the O_2 molecule,

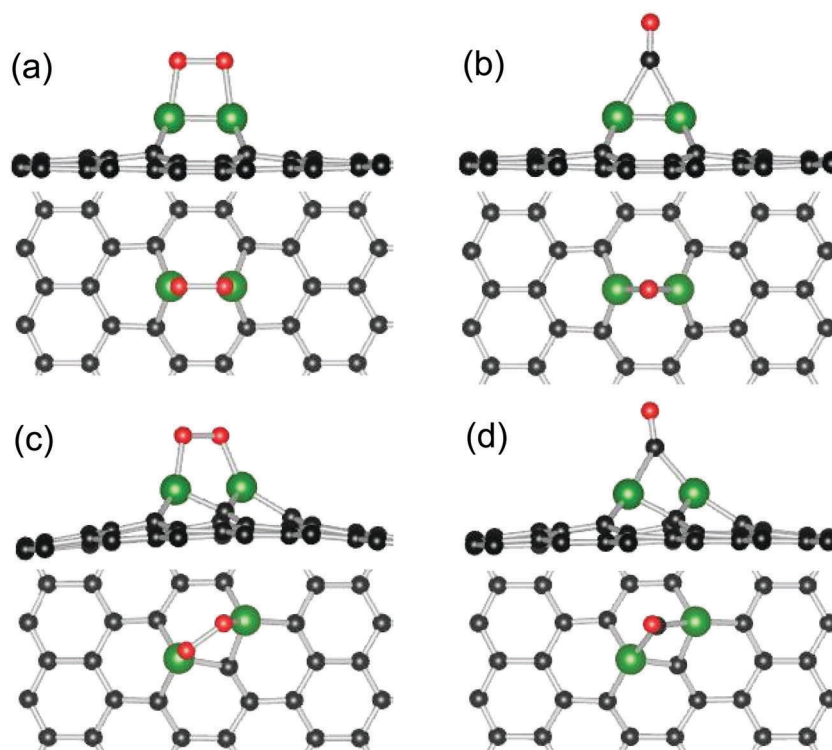


Fig. 2 Top and side views of the geometric structures of (a and c) O_2 and (b and d) CO adsorbed on (a and b) 2Fe-DG and (c and d) 2Fe-MG sheets. The green, black and red balls represent Fe, C and O atoms, respectively.

Table 1 Binding energies (E_{bind} in eV), bond lengths (d_1 in Å), adsorption heights (d_2 in Å), and numbers of electrons (Δq in e) transferred from 2Fe dopants embedded in graphene sheets to adsorbed O_2 , CO, O and CO_2 species

System		E_{bind} (eV)	d_1 (Å)	Δq (e)	d_2 (Å)
2Fe-DG	O_2	3.25	1.47	1.02	1.82
	CO	1.43	1.18	0.50	2.04
	O	6.74		1.03	1.79
	CO_2	0.69	1.26	0.85	1.94
2Fe-MG	O_2	3.67	1.48	1.06	1.78
	CO	1.72	1.19	0.57	1.94–2.04
	O	6.80		1.05	1.80
	CO_2	0.82	1.26	0.89	2.04

the more elongated is the O–O bond.⁴⁸ As shown in Fig. 3(a), the broadened partial DOS (PDOS) of the 2Fe 3d states strongly hybridize with the O_2 $2\pi^*$, 5σ and 1π orbitals around the Fermi level (E_{F}) and also overlap with the TDOS, which illustrates that there are stronger interactions between the Fe-DG sheet and the

O_2 molecule. In addition, the hybridization between adsorbed O_2 molecules and Fe atoms induces a magnetic moment in the entire system due to the increase in the number of unpaired electrons, which results in asymmetry between the spin-up and spin-down channels of the systems.

As shown in Fig. 2(b) and (d), an end-on configuration is favored for a CO molecule on the 2Fe-graphene substrates. An end-on CO molecule on a 2Fe-MG sheet has a higher E_{bind} value (1.72 eV) than on a 2Fe-DG sheet (1.43 eV). The adsorbed CO molecule is nearly vertical on the 2Fe-DG surface with the distance (d_2) between the Fe atom and CO molecule of 2.04 Å, while it is somewhat tilted on the 2Fe-MG surface with a Fe–CO distance of about 1.94–2.04 Å. The DOS plots for the adsorbed CO molecule on the 2Fe-DG system are shown in Fig. 3(b). Strong hybridization between the PDOS of the Fe 3d states and the CO $2\pi^*$, 5σ and 1π orbitals is observed around the E_{F} value. On the basis of Bader analysis, about 0.50 electrons are transferred from the 2Fe-DG sheet to the CO molecule, which occupy the CO $2\pi^*$ states and subsequently lead to an increase

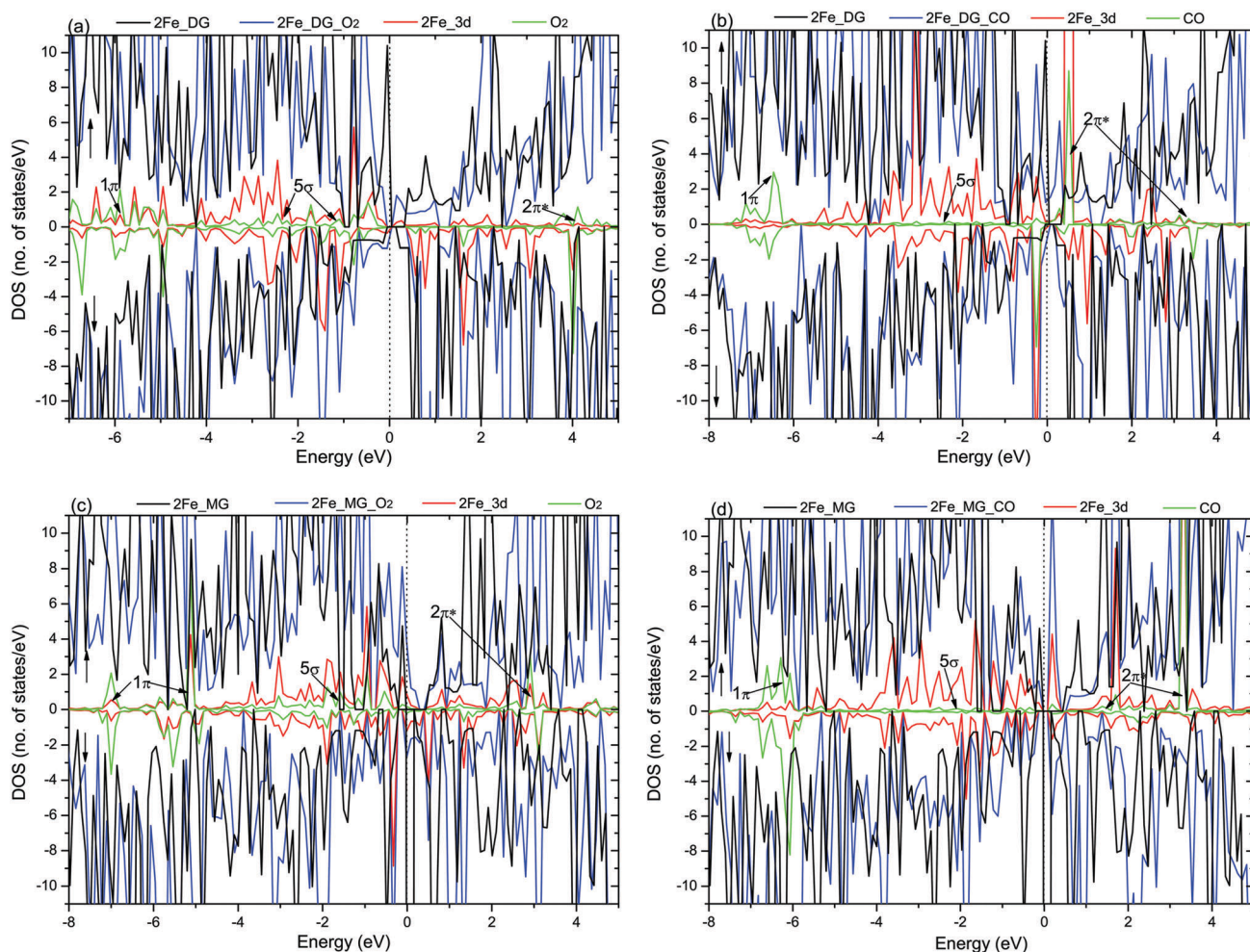


Fig. 3 Spin-resolved TDOS, local DOS (LDOS), and PDOS (spin-up labeled with \uparrow and spin-down labeled with \downarrow) for (a and c) O_2 and (b and d) CO adsorbed on (a and b) 2Fe-DG and (c and d) 2Fe-MG sheets. The black, blue and red solid curves represent the TDOS of 2Fe-DG (or 2Fe-MG) without (with) adsorbed O_2 (or CO) and the PDOS of the 2Fe 3d states with adsorbed O_2 (or CO), respectively, and the green solid curves represent the LDOS of adsorbed O_2 (or CO). The vertical dotted line denotes the Fermi level.

in the C–O bond length to 1.18 Å. In comparison, the adsorbed CO molecule on the 2Fe-MG surface gains more electrons (0.57 e) and the C–O bond length increases to 1.19 Å.

To gain more insight into the origin of the electronic properties of 2Fe-graphene sheets with adsorbed species, we investigated the DOS plots for O₂ and CO molecules on 2Fe-DG (or 2Fe-MG) systems, as shown in Fig. 3. The TDOS and PDOS plots for the 2Fe-graphene systems were clearly altered after the gas molecules were adsorbed. The DOS plots for the 2Fe-MG sheet with O₂ and CO molecules were comparatively studied, as shown in Fig. 3(c) and (d). In comparison with the bare 2Fe-MG sheet, the adsorption of O₂ introduces a significant shift in the DOS plots for the spin-up and spin-down channels. Spin-resolved DOS peaks appeared at the E_F value owing to the transfer of electrons from the 2Fe-MG sheet to the O₂ molecule, which illustrates that the adsorbed O₂ molecule on the 2Fe-MG system exhibits metallic properties, whereas the adsorbed O₂ molecule on the 2Fe-DG system has a small band gap and exhibits semiconducting properties. In the DOS plots for CO on the 2Fe-MG system, there is a band gap at the E_F value, and thus the semimetallic properties of the 2Fe-MG system are converted into semiconducting properties, as shown in Fig. 3(d). Besides, the broadened 2Fe 3d states strongly overlap with the LDOS of O₂ (or CO) and the TDOS of the system around the E_F value, which illustrates that strong hybridization could enhance the interactions between reactants and substrates. In comparison with the semimetallic properties of the 2Fe-DG system, a non-zero band gap is maintained in the spin-up channel and DOS peaks appear at the E_F value in the spin-down channel. CO adsorbed on the 2Fe-DG system thus exhibits metallic properties, as shown in Fig. 3(b). These results illustrate that the adsorption of CO and O₂ could effectively regulate the electronic properties of 2Fe-graphene systems, which could have a bearing on important applications in electronic and spintronic devices.

In order to understand the origin of the high stability of reactants on substrates, we investigated the valence charge distribution of an adsorbed O₂ (or CO) molecule on the 2Fe-graphene sheets as shown in Fig. 4. In comparison with the bare 2Fe-graphene systems, it was found that the adsorbed O₂ and CO molecules on the graphene sheets induce charge redistribution at their interfaces. As shown in Fig. 4(a) and (c), the charge density distribution and bond elongation of the O₂ molecule on 2Fe-MG (1.06 e , 1.48 Å) are more pronounced than those on 2Fe-DG (1.02 e , 1.47 Å), which indicates that the adsorption of O₂ on 2Fe-MG (3.67 eV) is stronger than that on 2Fe-DG (3.25 eV). In comparison, the adsorbed CO molecule gains fewer electrons (0.50 and 0.57 e) and exhibits lower stability (1.43 and 1.72 eV) on 2Fe-DG and 2Fe-MG as shown in Table 1. Besides, the greater number of electrons (> 2.0 e) transferred to the O₂ molecule on the 2Fe-graphene systems illustrates that O₂ is viewed as an electron-acceptor.⁴⁴ Bader charge analysis shows that in these systems the doped Fe atoms serve as donors for supplying electrons, which are partly transferred to the adsorbed gas molecules, whereas the rest are used to saturate the dangling bonds of carbon atoms, which illustrates that there exists bonding of covalent character

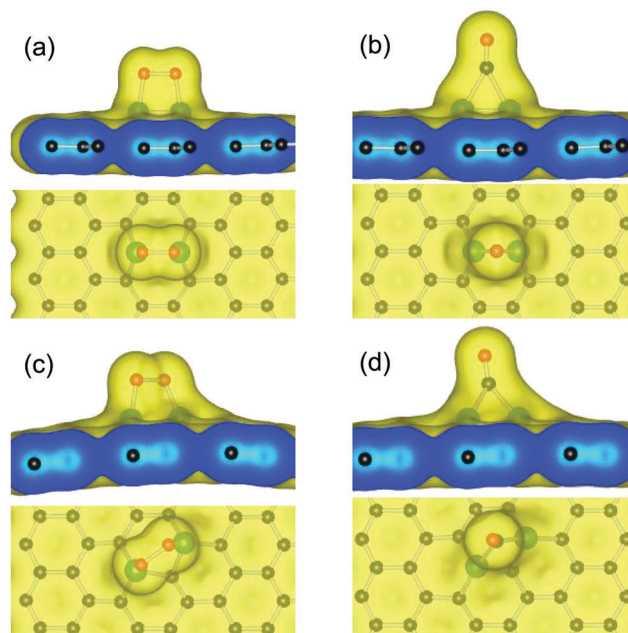


Fig. 4 Charge distribution for (a and c) O₂ and (b and d) CO adsorbed on (a and b) 2Fe-DG and (c and d) 2Fe-MG sheets. The contour lines in the plots are drawn at intervals of about 0.01 $e \text{ \AA}^{-3}$.

between adsorbates and substrates that facilitates their interaction. The lesser (or greater) accumulation of charge density between the CO (or O₂) molecule and the 2Fe-graphene sheet indicates that O₂ exhibits higher stability as an electron acceptor than CO and therefore more electrons are gained by the gas molecules and the adsorption becomes more stable.

As shown in Fig. 5, the adsorbed gas molecules (O₂ and CO) induce spin charge redistribution in the 2Fe-graphene substrates. It is observed that the more the electrons predominantly accumulate in the vicinity of the O₂–2Fe and CO–2Fe interfaces, the fewer are the electrons located on the neighboring carbon atoms of the graphene sheets. In comparison with the bare 2Fe-DG sheet (14.0 μ_B), the number of spin electrons on the Fe atoms greatly decreases due to the transfer of electrons from 2Fe-DG to the adsorbed gases and thus the O₂ (or CO) molecule on the 2Fe-DG system exhibits a lower magnetic moment (12.0 μ_B) as shown in Fig. 5(a) and (b). In comparison with the adsorption of CO on the 2Fe-MG system (10.0 μ_B), there is a more pronounced spin charge distribution in the O₂ molecule adsorbed on the 2Fe-MG system, which exhibits stronger magnetic properties (11.0 μ_B), whereas the magnetic moments of both systems are lower than that of the bare 2Fe-MG system (12.0 μ_B). In general, the magnetic moments of the 2Fe-graphene systems decrease when a gas molecule is adsorbed, because the transferred electrons induce spin charge redistribution between the substrate and adsorbate and reduce the number of unpaired electrons in the system. Hence, we could distinguish the type of gas adsorbed on a graphene-based device by measuring the change in the magnetic moment of the system. On the basis of the above discussions, it was found that the higher E_{bind} value of the O₂ molecule on the 2Fe-DG (2Fe-MG) sheet indicates semi-metallic

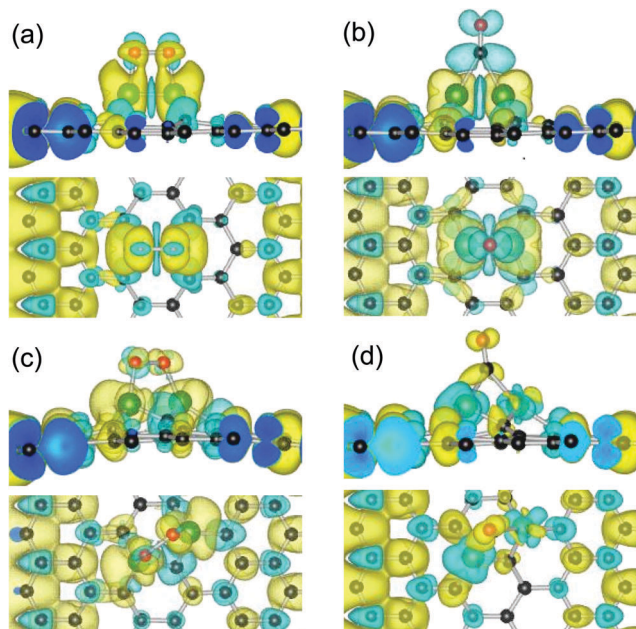


Fig. 5 Spin charge density plots for (a and c) O_2 and (b and d) CO adsorbed on (a and b) 2Fe-DG and (c and d) 2Fe-MG sheets. The contour lines in the plots are drawn at intervals of about $0.001 e \text{ \AA}^{-3}$.

(or metallic) properties, but the relatively smaller E_{bind} value of the CO molecule on the 2Fe-DG (or 2Fe-MG) sheet indicates metallic (or semi-metallic) properties. According to the DOS plots, the spin-up and spin-down channels of adsorbed O_2 and CO molecules on the 2Fe-graphene systems become asymmetric and exhibit magnetic properties because the transferred electrons cause spin polarization. Therefore, the spin charge distribution and magnetic properties of 2Fe-graphene systems could be regulated by selecting the appropriate adsorbed species.

3.3. CO oxidation reactions on 2Fe-graphene substrates

In general, the stability of gas molecules determines the reaction pathway on a catalyst.⁷³ Therefore, it is necessary to discuss the interactions between the active sites of catalysts and adsorbed gases. The above results show that the adsorbed O_2 molecule on the 2Fe-graphene systems tends to gain more electrons and exhibits higher stability than the CO molecule. The large energy difference between the individual gas molecules indicates that 2Fe-graphene is preferentially covered by adsorbed O_2 if a mixture of CO and O_2 is injected as the reaction gas and consequently CO will react with the preadsorbed O_2 . In addition, the high stability of the O_2 molecule on 2Fe-graphene together with the elongated O–O bond could indicate that the dissociation of O_2 is the initial step. Hence, the adsorbed O_2 is effectively activated, which holds promise for further CO oxidation reactions. In addition, the E_{bind} values of CO_2 on 2Fe-graphene (0.69 and 0.82 eV) are lower than those of the adsorbed CO and O_2 molecules, which suggest that a CO_2 molecule is more easily desorbed from the active site of the catalyst. The adsorbed O atom exhibits high stability at a bridging position on the Fe–Fe bond with high E_{bind} values (6.74 and 6.80 eV). Therefore, it is

worthwhile to study catalytic processes on 2Fe-graphene sheets by selecting different reaction mechanisms of CO oxidation.

3.3.1 Reaction pathways on 2Fe-DG sheet. There are two well-established mechanisms for CO oxidation with O_2 , namely, the Langmuir–Hinshelwood (LH) and Eley–Rideal (ER) mechanisms.^{20,30,45} The LH mechanism involves the coadsorption of CO and O_2 molecules before the reaction, followed by the formation of a peroxo-type $OOCO$ intermediate state (MS) and then the desorption of CO_2 molecule. In the ER mechanism, a gas-phase CO molecule directly reacts with an activated O_2 molecule (or atomic O) to produce a carbonate-like state CO_3 (or CO_2). In our study, several co-adsorbed configurations from the LH mechanism were tested. Initially, O_2 and CO molecules were placed at sites in close proximity. However, no $OOCO$ intermediate state was found after full geometry optimization, which is in accordance with the reported results.⁵⁷ This result indicates that the reaction process of CO oxidation on 2Fe-graphene *via* the LH mechanism is almost impossible or proceeds with great difficulty. Furthermore, the dissociative adsorption of O_2 molecules on 2Fe-graphene was also analyzed, which could provide a sufficient number of oxygen atoms, and the atomic O (O_{ads}) that is generated is active for the oxidation of CO *via* the ER mechanism. Therefore, the following steps in the oxidation of CO *via* the ER mechanism will be discussed later.

First, the dissociation of O_2 molecule on 2Fe-DG was studied as the first step (Fig. 6(a)) in which the most stable adsorbed configuration of O_2 is the IS and the two chemisorbed O atoms located on the top sites of the Fe atoms is the FS. During the reaction processes, the O–O bond is elongated from 1.47 to 3.32 Å and the calculated energy barrier of the dissociation of O_2 is 0.20 eV, which is much lower than that on Al-MG⁴⁵ and Fe-MG sheets.⁵⁸ This result illustrates that the doped Fe dimer as the active site is activated for the decomposition of O_2 . Then, we also determined whether the generated O_{ads} atoms participate in the oxidation of CO (IS, TS and FS) on the 2Fe/DG surface, which includes a two-step process involving the interaction between two O atoms and two CO molecules. In the first step, the structure with a generated O_{ads} atom and an approaching CO molecule above the respective Fe atom is viewed as the IS1, in which the CO–O distance is 3.03 Å. It has been shown that the CO molecule gradually reaches and reacts with the O_{ads} atom *via* the ER mechanism with an E_{bar} value of 0.53 eV, as shown in Fig. 6(a). In the second step, the physisorbed CO molecule is close to the binding O_{ads} atom, and the corresponding CO–O distance is 2.91 Å. When the carbon atom of the CO molecule approaches the O atom, a second CO_2 molecule is then generated with an E_{bar} value of 0.23 eV, which is lower than that in the first step. In the catalytic reactions, it was found that the dissociative adsorption of the O_2 molecule (0.20 eV) is energetically more favored than the CO_2 formation reactions (0.53 and 0.23 eV).

Secondly, the physisorbed CO molecule directly reacts with the preadsorbed O_2 molecule *via* the ER mechanism ($CO + O_2 \rightarrow CO_3$), and the corresponding optimized structures of each state along the MEP are shown in Fig. 6(b). Initially, the configuration in which the CO molecule is suspended above the preadsorbed O_2 molecule on the 2Fe-DG sheet is viewed as

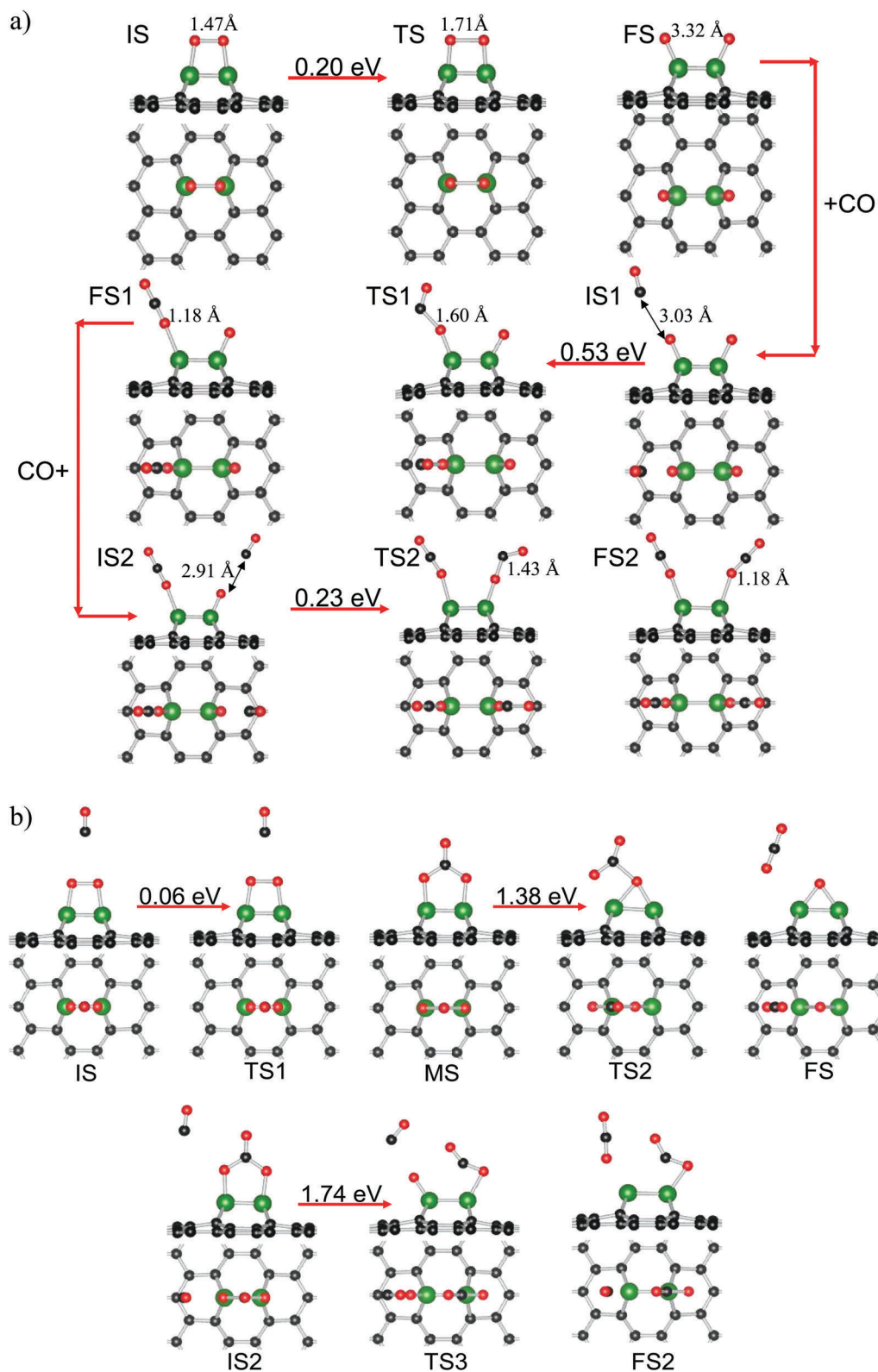


Fig. 6 Minimum energy profiles and configurations of different states in CO oxidation reactions on a 2Fe-DG sheet, including (a) the dissociative adsorption of an O_2 molecule and the $2CO + 2O_{ads}$ reaction and (b) the $CO + O_2$ and $CO_3 + CO$ reactions in the ER mechanism. The red, green, and black balls represent O, Fe and C atoms, respectively.

the IS. Subsequently, the CO molecule approaches the activated O_2 molecule and could be inserted into the O–O bond to form a CO_3 complex as an intermediate state (MS). The energy barrier of this reaction was calculated to be 0.06 eV (TS1). In the

reaction process, the C–O bond in CO is elongated from 1.14 to 1.21 Å and the O–O bond in O₂ is elongated from 1.45 to 2.27 Å. Then, the reaction could proceed *via* the dissociation of the CO₃ complex into a CO₂ molecule, which leaves an O atom (FS). The energy barrier (TS2) of this process is estimated to be 1.38 eV, which is much higher than that of the formation of the CO₃ complex and a similar reaction on an Mo-MG sheet.⁷⁴ Besides, the reversible reaction (CO₂ + O_{ads} → CO₃) has a much lower energy barrier (0.33 eV) in comparison with the dissociation of the CO₃ complex, which illustrates that the CO₃ complex is

more stable than the final products (CO₂ and O_{ads}) as shown in Fig. 6(b). Furthermore, in a possible reaction pathway the CO₃ complex reacts with a second CO molecule (IS2) to produce two CO₂ molecules (FS2) through the TS3, which has a higher energy barrier (1.74 eV) than that of the TS2. Although the formation of the CO₃ complex on the 2Fe-DG sheet has a much lower energy barrier, the system would be trapped by the CO₃ complex, and the generation of CO₂ is an energetically unfavored reaction.

On the basis of the above discussions, the dissociative adsorption of O₂ as an initial step is an energetically favored

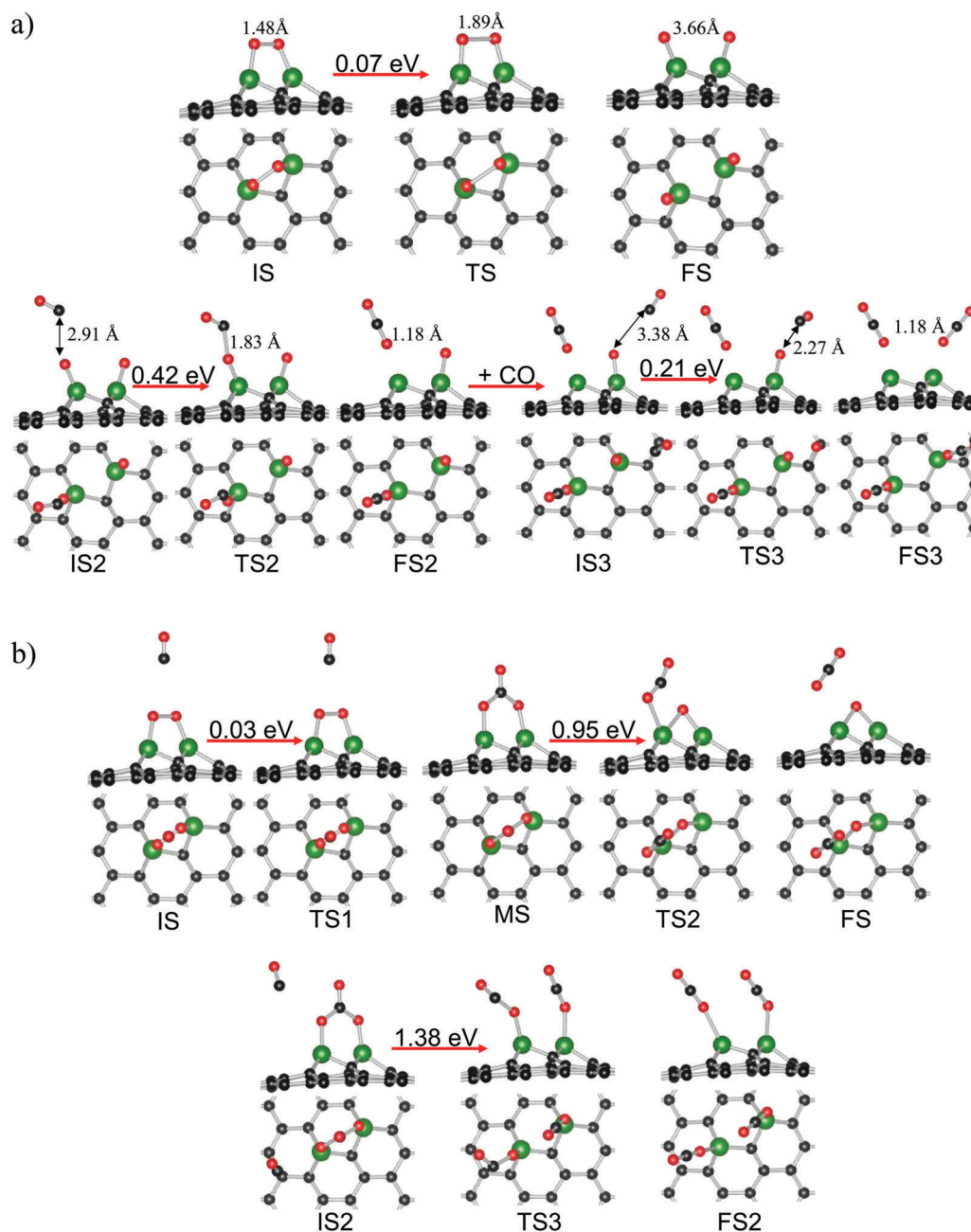


Fig. 7 Minimum energy profiles and configurations of different states in CO oxidation reactions on a 2Fe-MG sheet, including (a) the dissociative adsorption of an O₂ molecule and the 2CO + 2O_{ads} reaction and (b) the CO + O₂ and CO₃ + CO reactions in the ER mechanism. The red, green, and black balls represent O, Fe and C atoms, respectively.

reaction for CO oxidation, because the corresponding CO oxidation reactions have relatively low energy barriers (<0.6 eV), including the dissociation of the O₂ molecule and the reaction of two O_{ads} atoms with two CO molecules to form two CO₂ molecules.

3.3.2 Reaction pathways on 2Fe-MG sheet. In order to investigate the reaction mechanisms of CO oxidation on different 2Fe-graphene substrates, the relationship between the adsorption stability and the reaction pathways among the reactants and substrates was studied. The calculated results show that the individual CO and O₂ molecules on the 2Fe-MG sheet have higher E_{bind} values and energy differences than those on the 2Fe-DG sheet, which could affect the catalytic efficiency of CO oxidation. As shown in Fig. 7, the reaction pathways and energy barriers for CO oxidation on the 2Fe-MG sheet were investigated through the ER reaction mechanism, which includes the dissociation of O₂ and the formation of the CO₃ complex. First, the dissociation of O₂ as an initial step was studied (Fig. 7(a)). In this reaction, the O–O bond is elongated from 1.48 to 3.66 Å, and the generated O_{ads} atoms are anchored to the two Fe atoms. It was found that this reaction has an energy barrier of 0.07 eV *via* the TS, which is much lower than that on the 2Fe-DG sheet. We also determined whether the generated O_{ads} atom initially reacts with the physisorbed CO molecule, where the CO–O distance is 2.91 Å. It was shown that the CO molecule gradually reaches the O_{ads} atom and generates the first CO₂ molecule through the ER mechanism with an energy barrier of 0.42 eV (TS2). In the next step, the second CO molecule is close to the binding O_{ads} atom, and the TS3 is generated with a CO–O_{ads} distance of 3.38 Å (Fig. 7(a)). The second CO₂ molecule is formed with a lower energy barrier (0.21 eV) than that of the first step. In the reaction sequence, it was found that the dissociative adsorption of the O₂ molecule (0.07 eV) is more favored than those of the formed CO₂ molecules (0.42 and 0.21 eV). In comparison, the catalytic CO oxidation reactions on the 2Fe-MG sheet need to overcome lower energy barriers than those on the 2Fe-DG sheet.

To gain a better understanding of the CO oxidation reactions through ER mechanism, the formation of the carbonate-like (CO₃) complex as an initial step was also studied, and the corresponding reaction processes are shown in Fig. 7(b). First, the configuration in which the physisorbed CO molecule is located above the preadsorbed O₂ molecule on the 2Fe-MG sheet was selected as the IS. On approaching the activated O₂ molecule, one CO molecule could be inserted into the O–O bond to form a CO₃ complex on the Fe atoms with a much lower energy barrier of 0.03 eV (TS1). Then, the reaction could proceed *via* the dissociation of the CO₃ complex into a CO₂ molecule, which leaves an O_{ads} atom (FS). This process needs to overcome a high energy barrier (TS2) of 0.95 eV, which is similar to that on the 2Fe-DG sheet. Furthermore, in another reaction pathway the CO₃ complex reacts with a second CO molecule to form two CO₂ molecules through the TS3. In this reaction (CO₃ + CO → 2CO₂), the calculated energy barrier (1.38 eV) is higher than that of the dissociation of the CO₃ complex (0.95 eV), which indicates that the presence of the CO molecule is unfavorable for the dissociation of the CO₃ complex.

It was concluded that the dissociation of the CO₃ complex proceeds with great difficulty and that the CO₃ complex formed on 2Fe-MG is more stable than the final products. Hence, the formation of the carbonate-like (CO₃) complex *via* the ER mechanism is an energetically unfavored process.

For the CO oxidation reactions on the 2Fe-graphene sheets, it was found that the dissociation reactions of O₂ molecules have lower energy barriers (<0.2 eV) than the subsequent reactions between O_{ads} and CO molecules in the ER mechanism (2CO + 2O → 2CO₂). Although the formation of the CO₃ complex as the initial step has a much lower energy barrier, the carbonate-like CO₃ complex directly dissociates to produce a physisorbed CO₂ molecule with a higher energy barrier. Therefore, the catalytic CO oxidation reaction on the 2Fe-graphene sheets through the ER mechanism is almost impossible or proceeds with great difficulty. In comparison, the dissociative adsorption of the O₂ molecule directly generates two O_{ads} atoms with a low energy barrier, which is also lower than those on Fe-doped graphene⁵⁸ and Si-GN4 sheets.⁷⁵ In comparison with single-atom catalysts, the use of two Fe atoms as the active sites could enhance the interaction between O₂ molecules and the graphene substrate because with increase in the number of electrons transferred, the O–O bond is more easily broken and the generated O atoms are active for the oxidation through ER mechanism. In light of the aforementioned discussion, it could be concluded that the sequential reactions of CO oxidation on the 2Fe-graphene substrates through the similar reaction processes (including O₂ → 2O_{ads} and 2CO + 2O_{ads} → 2CO₂) have sufficiently low energy barriers (<0.6 eV) and are more likely to proceed rapidly in practical reactions. Therefore, 2Fe-graphene substrates exhibit high activity in the catalytic CO oxidation reaction and provide a valuable reference for understanding the reaction mechanism and designing functionalized graphene-based devices.

4. Conclusions

The first-principles calculations were performed to investigate the geometric and electronic properties of 2Fe-graphene systems. It was found that a 2Fe-DG sheet is more stable than a 2Fe-MG sheet, and positively charged Fe dopants could effectively regulate the stability of adsorbed species. In comparison with an adsorbed CO molecule, the high adsorption energy and elongated O–O bond of an O₂ molecule on the 2Fe-graphene sheets indicate that the dissociation of O₂ is the more favored process. In addition, the catalytic CO oxidation reactions on the 2Fe-MG and 2Fe-DG sheets were investigated comparatively through different reaction mechanisms. In the ER mechanism, a preadsorbed O₂ molecule reacts with a CO molecule to form a CO₃ complex with a much lower energy barrier, but the CO₃ complex is more stable than the final products. In comparison, the dissociative adsorption of an O₂ molecule as the initial reaction, followed by the subsequent ER reactions (2CO + 2O_{ads} → 2CO₂) are more likely to proceed rapidly on the Fe-graphene sheets because these catalytic processes have sufficiently low energy barriers. The results obtained in our study demonstrate that the 2Fe-graphene sheets are promising anode materials for

CO oxidation and could help in the fabrication of graphene-based catalysts with low cost and high activity.

Conflicts of interest

There are no conflicts to declare.

Acknowledgements

This study was supported by the National Natural Science Foundation of China (Grant No. U1404109, 11504334, 11791240177, 11704005 and 61674053), the Natural Science Foundation of Henan Province (Grant No. 162300410325) and Sponsored by Program for Science & Technology Innovation Talents in Universities of Henan Province (Grant No. 18HASTTT030).

References

- 1 A. Alavi, P. Hu, T. Deutsch, P. L. Silvestrelli and J. Hutter, *Phys. Rev. Lett.*, 1998, **80**, 3650–3653.
- 2 M. Ackermann, T. Pedersen, B. Hendriksen, O. Robach, S. Bobaru, I. Popa, C. Quiros, H. Kim, B. Hammer, S. Ferrer and J. W. M. Frenken, *Phys. Rev. Lett.*, 2005, **95**, 255505.
- 3 C. Zhang and P. Hu, *J. Am. Chem. Soc.*, 2001, **123**, 1166–1172.
- 4 A. A. Herzog, C. J. Kiely, A. F. Carley, P. Landon and G. J. Hutchings, *Science*, 2008, **321**, 1331–1335.
- 5 X. Xie, Y. Li, Z. Q. Liu, M. Haruta and W. Shen, *Nature*, 2009, **458**, 746–749.
- 6 V. Shapovalov and H. Metiu, *J. Catal.*, 2007, **245**, 205–214.
- 7 X. Q. Gong, Z. P. Liu, R. Raval and P. Hu, *J. Am. Chem. Soc.*, 2004, **126**, 8–9.
- 8 Z. P. Liu, X. Q. Gong, J. Kohanoff, C. Sanchez and P. Hu, *Phys. Rev. Lett.*, 2003, **91**, 266102.
- 9 L. Molina and B. Hammer, *Phys. Rev. Lett.*, 2003, **90**, 206102.
- 10 B. Qiao, A. Wang, X. Yang, L. F. Allard, Z. Jiang, Y. Cui, J. Liu, J. Li and T. Zhang, *Nat. Chem.*, 2011, **3**, 634–641.
- 11 G. Chen, S. J. Li, Y. Su, V. Wang, H. Mizuseki and Y. Kawazoe, *J. Phys. Chem. C*, 2011, **115**, 20168–20174.
- 12 W. An and P. Liu, *Phys. Chem. Chem. Phys.*, 2016, **18**, 30899–30902.
- 13 W. Ju, T. Li, X. Su, H. Li, X. Li and D. Ma, *Phys. Chem. Chem. Phys.*, 2017, **19**, 20735–20748.
- 14 C. Chang, C. Cheng and C. Wei, *J. Chem. Phys.*, 2008, **128**, 124710.
- 15 N. Lopez and J. K. Nørskov, *J. Am. Chem. Soc.*, 2002, **124**, 11262–11263.
- 16 B. Kalita and R. C. Deka, *J. Am. Chem. Soc.*, 2009, **131**, 13252–13254.
- 17 Y. XiaoFeng, W. AiQin, Q. Botao, L. Jun, L. Jingyue and Z. Tao, *Acc. Chem. Res.*, 2013, **46**, 1740–1748.
- 18 I. N. Remediakis, N. Lopez and J. K. Nørskov, *Angew. Chem., Int. Ed.*, 2005, **44**, 1824–1826.
- 19 Z. Lu, P. Lv, Y. Liang, D. Ma, Y. Zhang, W. Zhang, X. Yang and Z. Yang, *Phys. Chem. Chem. Phys.*, 2016, **18**, 21865–21870.
- 20 L.-Y. Feng, Y.-J. Liu and J.-X. Zhao, *J. Power Sources*, 2015, **287**, 431–438.
- 21 K. Mao, L. Li, W. Zhang, Y. Pei, X. C. Zeng, X. Wu and J. Yang, *Sci. Rep.*, 2014, **4**, 5441.
- 22 E. Antolini, *Appl. Catal., B*, 2012, **123–124**, 52–68.
- 23 C. Lee, X. Wei, J. W. Kysar and J. Hone, *Science*, 2008, **321**, 385–388.
- 24 J. Zhang, S. Tang, L. Liao, W. Yu, J. Li, F. Seland and G. M. Haarberg, *J. Power Sources*, 2014, **267**, 706–713.
- 25 A. A. Balandin, S. Ghosh, W. Bao, I. Calizo, D. Teweldebrhan, F. Miao and C. N. Lau, *Nano Lett.*, 2008, **8**, 902–907.
- 26 M. Zhou, A. Zhang, Z. Dai, C. Zhang and Y. Feng, *J. Chem. Phys.*, 2010, **132**, 194704.
- 27 I. Fampiou and A. Ramasubramaniam, *J. Phys. Chem. C*, 2015, **119**, 8703–8710.
- 28 B. F. Machado and P. Serp, *Catal. Sci. Technol.*, 2012, **2**, 54–75.
- 29 N. G. Sahoo, Y. Pan, L. Li and S. H. Chan, *Adv. Mater.*, 2012, **24**, 4203–4210.
- 30 K. Chan, J. Neaton and M. Cohen, *Phys. Rev. B: Condens. Matter Mater. Phys.*, 2008, **77**, 235430.
- 31 Y. Zhou, X. Zu, F. Gao, H. Lv and H. Xiao, *Appl. Phys. Lett.*, 2009, **95**, 123119.
- 32 M. Wu, E. Liu and J. Jiang, *Appl. Phys. Lett.*, 2008, **93**, 082504.
- 33 M. Wu, E. Liu, M. Ge and J. Jiang, *Appl. Phys. Lett.*, 2009, **94**, 102505.
- 34 Y. N. Tang, Z. X. Yang and X. Q. Dai, *J. Magn. Magn. Mater.*, 2011, **323**, 2441–2447.
- 35 W. Ju, T. Li, H. Wang, Y. Yong and J. Sun, *Chem. Phys. Lett.*, 2015, **622**, 109–114.
- 36 Q. Tang, Z. Zhou and Z. Chen, *Nanoscale*, 2013, **5**, 4541–4583.
- 37 A. Krasheninnikov, P. Lehtinen, A. Foster, P. Pyykkö and R. Nieminen, *Phys. Rev. Lett.*, 2009, **102**, 126807.
- 38 E. J. G. Santos, A. Ayuela and D. Sánchez-Portal, *New J. Phys.*, 2010, **12**, 053012.
- 39 Y. N. Tang, Z. X. Yang and X. Q. Dai, *J. Chem. Phys.*, 2011, **135**, 224704.
- 40 H. Wang, Q. Wang, Y. Cheng, K. Li, Y. Yao, Q. Zhang, C. Dong, P. Wang, U. Schwingenschlöggl, W. Yang and X. X. Zhang, *Nano Lett.*, 2012, **12**, 141–144.
- 41 A. Ambrosi, S. Y. Chee, B. Khezri, R. D. Webster, Z. Sofer and M. Pumera, *Angew. Chem., Int. Ed.*, 2012, **51**, 500–503.
- 42 E. H. Song, Z. Wen and Q. Jiang, *J. Phys. Chem. C*, 2011, **115**, 3678–3683.
- 43 Y. Lu, M. Zhou, C. Zhang and Y. Feng, *J. Phys. Chem. C*, 2009, **113**, 20156–20160.
- 44 Y. Tang, Z. Yang and X. Dai, *Phys. Chem. Chem. Phys.*, 2012, **14**, 16566–16572.
- 45 Q. G. Jiang, Z. M. Ao, S. Li and Z. Wen, *RSC Adv.*, 2014, **4**, 20290–20296.
- 46 Y. Tang, X. Dai, Z. Yang, Z. Liu, L. Pan, D. Ma and Z. Lu, *Carbon*, 2014, **71**, 139–149.
- 47 L. Xin, S. Yanhui, D. Ting, M. Changong and H. Yu, *Phys. Chem. Chem. Phys.*, 2014, **16**, 23584–23593.
- 48 Y. Tang, Z. Yang, X. Dai, D. Ma and Z. Fu, *J. Phys. Chem. C*, 2013, **117**, 5258–5268.

- 49 M. N. Groves, C. Malardier-Jugroot and M. Jugroot, *J. Phys. Chem. C*, 2012, **116**, 10548–10556.
- 50 C. Cao, M. Wu, J. Jiang and H. Cheng, *Phys. Rev. B: Condens. Matter Mater. Phys.*, 2010, **81**, 205424.
- 51 H. Johll, H. C. Kang and E. S. Tok, *Phys. Rev. B: Condens. Matter Mater. Phys.*, 2009, **79**, 245416.
- 52 R. Varns and P. Strange, *J. Phys.: Condens. Matter*, 2008, **20**, 225005.
- 53 D. Ma, Z. Lu, W. Ju and Y. Tang, *J. Phys.: Condens. Matter*, 2012, **24**, 145501.
- 54 K. Wong, Q. Zeng and A. Yu, *Chem. Eng. J.*, 2011, **174**, 408–412.
- 55 L. Zhang, H. Y. Kim and G. Henkelman, *J. Phys. Chem. Lett.*, 2013, **4**, 2943–2947.
- 56 S. Dong, Y. Zhang, X. Zhang, J. Mao and Z. Yang, *Appl. Surf. Sci.*, 2017, **402**, 168–174.
- 57 Y. Li, Z. Zhou, G. Yu, W. Chen and Z. Chen, *J. Phys. Chem. C*, 2010, **114**, 6250–6254.
- 58 Y. Tang, J. Zhou, Z. Shen, W. Chen, C. Li and X. Dai, *RSC Adv.*, 2016, **6**, 93985–93996.
- 59 B. L. He, J. S. Shen and Z. X. Tian, *Phys. Chem. Chem. Phys.*, 2016, **18**, 24261–24269.
- 60 F. Li, J. Zhao and Z. Chen, *J. Phys. Chem. C*, 2012, **116**, 2507–2514.
- 61 Z. He, K. He, A. W. Robertson, A. I. Kirkland, D. Kim, J. Ihm, E. Yoon, G.-D. Lee and J. H. Warner, *Nano Lett.*, 2014, **14**, 3766–3772.
- 62 A. W. Robertson, B. Montanari, K. He, J. Kim, C. S. Allen, Y. A. Wu, J. Olivier, J. Neethling, N. Harrison and A. I. Kirkland, *Nano Lett.*, 2013, **13**, 1468–1475.
- 63 G. Kresse and J. Furthmüller, *Comput. Mater. Sci.*, 1996, **6**, 15–50.
- 64 G. Kresse and J. Furthmüller, *Phys. Rev. B: Condens. Matter Mater. Phys.*, 1996, **54**, 11169–11186.
- 65 G. Kresse and D. Joubert, *Phys. Rev. B: Condens. Matter Mater. Phys.*, 1999, **59**, 1758–1775.
- 66 J. Perdew, K. Burke and M. Ernzerhof, *Phys. Rev. Lett.*, 1996, **77**, 3865–3868.
- 67 J. Carlsson and M. Scheffler, *Phys. Rev. Lett.*, 2006, **96**, 46806.
- 68 G. Henkelman, A. Arnaldsson and H. Jónsson, *Comput. Mater. Sci.*, 2006, **36**, 354–360.
- 69 G. Henkelman, B. Uberuaga and H. Jónsson, *J. Chem. Phys.*, 2000, **113**, 9901–9904.
- 70 G. Henkelman and H. Jónsson, *J. Chem. Phys.*, 2000, **113**, 9978–9985.
- 71 J. A. Rodriguez-Manzo and F. Banhart, *Nano Lett.*, 2009, **9**, 2285–2289.
- 72 W. Orellana, *J. Phys. Chem. C*, 2013, **117**, 9812–9818.
- 73 H. Liu, B. Wang, M. Fan, N. Henson, Y. Zhang, B. F. Towler and H. G. Harris, *Fuel*, 2013, **113**, 712–718.
- 74 Y. Tang, L. Pan, W. Chen, C. Li, Z. Shen and X. Dai, *Appl. Phys. A: Mater. Sci. Process.*, 2015, **119**, 475–485.
- 75 Y. Tang, W. Chen, Z. Shen, S. Chang, M. Zhao and X. Dai, *Carbon*, 2017, **111**, 448–458.